An Ab Initio Study of the Low-Lying Electronic States of YO_2 and Franck−Condon Simulation of the First Photodetachment Band of YO_2^-

Edmond P. F. Lee,*,†,‡ John M. Dyke,‡ Daniel K. W. Mok,*,† and Foo-tim Chau†

Department of Applied Biology and Chemical Technology, The Hong Kong Polytechnic University, Hung Hom, Hong Kong, and School of Chemistry, University of Southampton, Highfield, Southampton, SO17 1BJ U.K.

Received: December 20, 2007; Revised Manuscript Received: February 22, 2008

A variety of density functional theory and ab initio methods, including B3LYP, B98, BP86, CASSCF, CASSCF/RS2, CASSCF/MRCI, BD, BD(T), and CCSD(T), with ECP basis sets of up to the quintuple-zeta quality for Y, have been employed to study the $\tilde{X}^2B_2$ state of YO_2 and the $\tilde{X}^1A_1$ state of YO_2^-. Providing that the Y $4s^24p^6$ outer-core electrons are included in the correlation treatment, the RCCSD(T) method gives the most consistent results and is concluded to be the most reliable and practical computational method for YO_2 and YO_2^-. In addition, RCCSD(T) potential energy functions (PEFs) of the $\tilde{X}^2B_2$ state of YO_2 and the $\tilde{X}^1A_1$ state of YO_2^- were computed, employing the ECP28MDF_aug-cc-pwCVTZ and aug-cc-pVTZ basis sets for Y and O, respectively. Franck−Condon factors, which include allowance for Duschinsky rotation and anharmonicity, were calculated using the computed RCCSD(T) PEFs and were used to simulate the first photodetachment band of YO_2^-. The simulated spectrum matches very well with the corresponding experimental 355 nm photodetachment spectrum of Wu, H.; Wang, L.-S. *J. Phys. Chem. A* 1998, *102*, 9129, confirming the reliability of the RCCSD(T) PEFs used. Further calculations on low-lying electronic states of YO_2 gave T_e's and T_{vert}'s of the $\tilde{A}^2A_1$, $\tilde{B}^2B_1$, and $\tilde{C}^2A_2$ states of YO_2, as well as EAs and VDEs to these states from the $\tilde{X}^1A_1$ state of YO_2^-. On the basis of the ab initio VDEs obtained in the present study, previous assignments of the second and third photodetachment bands of YO_2^- have been revised.

Introduction

Yttrium oxide has various novel industrial applications. For example, yttrium oxide is used in plasma spray deposition for coating crucibles and molds that handle highly reactive molten metals like uranium, titanium, chromium, beryllium, and their alloys[1] and in nanosized Er, Yb−yttrium oxide upconverters in emitting light devices (phosphors) and photonic-based telecommunication.[2] It is also used in yttria-doped alumina aerogel for the thermocatalytic cracking process of petroleum feedstocks,[3] in commercially available polycrystalline ceramic Nd^{3+}/Y_2O_3 and nanocrystalline aggregates of Nd^{3+}/Y_2O_3,[4] and as a buffer layer in the metal−ferroelectric insulator−semiconductor field effect transistor.[5] In view of its importance in various specialized applications, neutral and/or ionic clusters of yttrium oxide have been investigated recently by density functional theory (DFT) calculations,[6–8] pulsed laser vaporization time-of-flight mass spectrometry,[9,10] and photodetachment spectroscopy.[11,12]

In the present article, we focus on low-lying electronic states of YO_2 and the 355 nm (3.49 eV) photodetachment spectrum of YO_2^- published nearly 10 years ago.[11] The photodetachment spectrum of YO_2^- consists of four bands. On the basis of the electronic configuration of VO_2 obtained from previous CASSCF calculations[13] and by subtracting two valence electrons from VO_2, the four observed photodetachment bands of YO_2^- were assigned to detachments to the $\tilde{X}^2B_2$, $\tilde{A}^2B_1$, $\tilde{B}^2A_1$, and $\tilde{C}^2A_2$ states of YO_2 (see ref 11 for details). Among these four observed detachment bands, only the first one is vibrationally resolved. Three to four vibrational components with measured vibrational separations of 640 ± 80 cm^{-1} were observed, and they were assigned to excitation of the symmetric stretching mode (ν_1) of the $\tilde{X}^2B_2$ state of YO_2. In addition to this photodetachment study of ref 11, there is only one previous investigation, namely, a combined infrared (IR) matrix isolation and DFT study,[6] available on YO_2 and YO_2^-. The BP86 functional was employed in the DFT calculations, and the LanL2DZ basis set was used for Y, while the D95*, 6-31+G* and 6-311+G(3d) basis sets were used for O in ref 6. On the basis of computed DFT values, the observed vibrational frequencies of 702.0, 618.0, and 708.2 cm^{-1} in the IR spectra were assigned to ν_1 and ν_3 of YO_2^- and ν_1 of YO_2, respectively. EA values ranging from 41 to 46 kcal/mol (i.e., 1.78 to 1.99 eV, depending on the basis set used for O) were also derived from computed electronic energies of the $\tilde{X}^1A_1$ state of YO_2^- and the $\tilde{X}^2B_2$ state of YO_2 in ref 6. However, to our knowledge, no computational study has been carried out on low-lying excited states of YO_2.

It should be noted that the photodetachment spectrum of ScO_2^-, a lighter analogue of YO_2^-, was also published in ref 11. However, in contrast to YO_2 and YO_2^-, which have been studied computationally only by DFT using the BP89 functional mentioned above,[6] ScO_2 and/or ScO_2^- have been investigated by a variety of theoretical methods in a number of publications, including the {B3LYP, BP86, CASSCF, MP2, CCSD(T)},[14] {BP86, B3LYP, RCCSD(T), CASPT2},[15] (BPW91, BLYP, HFDFT),[16] {BP86, B3LYP, UHF/CCSD(T), ROHF/CCSD(T)},[17] and {UHF-MBPT(2), UHF-CCSD, UHF-CCSD(T), UHF-CCSDT, ROHF-MBPT(2), ROHF-CCSD, ROHF-CCSD(T), ROHF-CCSDT, B-CCSD and BCCD(T)}[18] methods. These calculations on ScO_2 and/or ScO_2^- will not be discussed here, as readers can refer to ref 18 and references therein for details. However, the number of calculations on ScO_2 and ScO_2^- listed highlights the immense interest in, and the high theoretical

* To whom correspondence should be addressed.
† The Hong Kong Polytechnic University.
‡ University of Southampton.

10.1021/jp711948r CCC: $40.75
Published on Web 04/18/2008

TABLE 1: Basis Sets Used for Y and O (*n* Refers to the Total Number of Contracted Basis Functions Used for YO_2 or YO_2^-)

	Y			
basis	ECP and basis set	remarks	O[a]	*n*
A	ECP28MWB[6s5p3d2f]	Stuttgart RSC 1997[b] + 2f[c]	AVDZ	96
B	ECP28MWB[6s5p3d2f]	as above	AVTZ (no f)	114
C	ECP28MWB(8s7p6d2f)	as above (uncontracted)	AVDZ	119
D	ECP28MHF(8s7p6d)[d] + 2f	uncontracted + 2f(0.1, 0.04)[e]	AVTZ (no f)	137
E	ECP28MWB[6s5p3d2f1g]	Stuttgart RSC 1997[b] + 2f1g[c]	AVTZ	151
F	ECP28MWB[6s5p3d][b] + 2f	augmented 2f(0.1, 0.04)[e]	6−311+G (2d)	104
G	ECP28MDF_AVTZ (no g)	AVTZ-PP[f] (no g)	AVTZ (no f)	134
H	ECP28MDF_AVTZ	AVTZ-PP[f]	AVTZ	180
I	ECP28MDF_AVQZ	AVQZ-PP[f]	AVQZ	295
J	ECP28MDF_wCVTZ	wCVTZ-PP[f]	ACVTZ	215
K	ECP28MDF_wCVQZ	wCVQZ-PP[f]	AVQZ	304
L	ECP28MDF_AwCVTZ[g]	wCVTZ-PP + aug(AVTZ-PP)	AVTZ	214
L1	ECP28MDF_AwCVTZ[g] (no g)	as above, but no g functions	AVTZ (no f)	159
M	ECP28MDF_wCV5Z	wCV5Z-PP[f]	AV5Z	460

[a] Standard aug-cc-pVDZ (AVDZ), aug-cc-pVTZ (AVTZ), aug-cc-pVQZ (AVQZ), and aug-cc-pCVTZ (ACVTZ) basis sets were used for O. [b] The [6s5p3d] basis set and the small core quasi-relativistic ECP, ECP28MWB, correspond to revision: Fri Jun 27 1997 of the Stuttgart/Dresden groups. This is also known as the Stuttgart RSC (relativistic small core) ECP basis set; see the earlier reference 21. [c] The contracted [6s5p3d2f1g] basis set is from the MOLPRO basis set library with the ECP28MWB ECP and is the same as that given on the Stuttgart website;[20] see also refs 22 and 23. The [6s5p3d] part is the same as the Stuttgart RSC 1997 basis set. [d] The uncontracted s, p, and d functions of the ECP28MHF basis set are from the MOLPRO basis set library. [e] Augmented 2f functions and their exponents. [f] The AVTZ-PP, AVQZ-PP, wCVTZ-PP, wCVQZ-PP, and wCV5Z-PP basis sets are from the Stuttgart Web site[20] and employ the small core fully relativistic ECP, ECP28MDF.[19] [g] The aug-part of the AVTZ-PP was added to the wCVTZ-PP basis set to give the AwCVTZ-PP basis set.

demands on the calculations of, this type of transition-metal oxide systems.

Last, it should be noted that, very recently, valence basis sets of the aug-cc-pVXZ and cc-pwCVXZ types, which couple with the fully relativistic effective core potential (ECP), ECP28MDF, have been published for second-row transition metals, including Y.[19,20] The availability of these high-quality ECP basis sets facilitates higher level ab initio calculations on second-row transition-metal oxides than those previously possible, and we have also employed these basis sets in the present investigation, as described in the following section.

Theoretical Considerations and Computational Details

Ab Initio Calculations. Table 1 summarizes the basis sets used in the present study. Basis sets A−F are based on the earlier quasi-relativistic small core (RSC) ECP basis set (except basis set D, which has employed the nonrelativistic ECP, ECP28MHF) of the Stuttgart group for Y,[21−23] while basis sets G−M consist of the recently available, fully relativistic augmented correlation-consistent polarized valence (aug-cc-pVXZ-PP or AVXZ-PP; see the Stuttgart website[20]), or polarized weighted core-valence (cc-pwCVXZ-PP or wCVXZ-PP), ECP basis sets mentioned above for Y.[19,20] Corresponding basis sets of similar qualities to those of Y have been used for O and are also given in Table 1. In general, smaller basis sets were employed for DFT along with computationally more demanding calculations {e.g., BD, BD(T) and multireference calculations; vide infra}, while larger basis sets were used for RCCSD(T) calculations. In order to examine basis set effects on computed quantities, basis set variations involve changing emphases on different parts of the basis set (e.g., uncontracting the Stuttgart RSC basis set for Y and/or changing the basis set of O) and/or a systematic improvement in the basis size/quality (e.g., employing the cc-pwCVXZ-PP-type basis sets for Y and corresponding aug-cc-pVXZ basis sets for O, with X = T, Q, or 5). It should be mentioned particularly that the cc-pwCVXZ-PP (X = T, Q, or 5) basis sets of Y, which include additional sets of tight functions (cf. aug-cc-pVXZ-PP), were designed for accounting adequately for the explicit correlation of the Y $4s^24p^6$ electrons.

Three functionals were employed in DFT calculations, namely, B3LYP, BP86 (or B88−P86, i.e., the Becke 88 exchange functional[24] coupled with the Perdew 86 correlation functional[25]), and B98.[26] DFT calculations, particularly employing these three functionals, were carried out because it has been reported that DFT calculations employing these functionals on some transition-metal oxides gave reliable results.[6,8,14,16] In addition to DFT calculations, CASSCF,[27] CASSCF/RSPT2 (multireference Rayleigh−Schrodinger perturbation theory to the second order[28,29] as implemented in the MOLPRO suite of programs[30]), CASSCF/MRCI,[31] RCCSD(T),[32] RHF/UCCSD(T),[33] UHF/CCSD(T),[34,35] and BD and BD(T) (Brueckner doubles plus noniterative triple contributions[36] as implemented in the GAUSSIAN03 suite of programs[37]) calculations were also carried out.

First, it should be noted that, for the open-shell $\tilde{X}^2B_2$ state of YO_2, calculations performed with GAUSSIAN03 have employed unrestricted-spin wave functions. These include DFT, CCSD(T), BD, and BD(T) calculations. With MOLPRO, the DFT calculations are also unrestricted-spin (i.e., UKS; see MOLPRO user manual[38]), but CASSCF, CASSCF/RSPT2, CASSCF/MRCI, and RCCSD(T) calculations are restricted-spin. In addition, UCCSD(T) calculations with MOLPRO, which employ restricted-spin open-shell Hartree−Fock wave functions (ROHF; see ref 33 and MOLPRO user manual) have also been performed. Nevertheless, RHF/UCCSD(T) results were found to be almost identical to RCCSD(T) results using the same basis set for both the $\tilde{X}^1A_1$ state of YO_2^- and the $\tilde{X}^2B_2$ state of YO_2.

Second, with the ECPs used in the present study for Y (see Table 1), the $1s^22s^22p^63s^23p^63d^{10}$ electrons of Y (i.e., 28 core electrons) are accounted for by the ECPs, and the Y $4s^24p^64d^15s^2$ electrons are considered as valence. However, it should be noted that with GAUSSIAN03, the default frozen core used in correlated calculations consists of only the O $1s^2$ electrons, while the default frozen core with MOLPRO consists of the O $1s^2$ and also the Y $4s^24p^6$ electrons. Nevertheless, the Y $4s^24p^6$ electrons were also explicitly correlated in some RCCSD(T) calculations using MOLPRO (vide infra).

Third, CASSCF calculations and post-CASSCF calculations were found to be computationally very demanding. For instance, with the default frozen core of O $1s^2$ and Y $4s^24p^6$ used by MOLPRO, that is, with an active space consisting of the O 2s2p and Y 5s4d shells, the CASSCF/H calculation on the $\tilde{X}^1A_1$ state of YO_2^- has over 2.25 million variables. For the CASSCF/MRCI/G calculation on the $\tilde{X}^2B_2$ state of YO_2, with the frozen core of O $1s^22s^2$ and Y $4s^24p^6$ (i.e., with closed,4,1,3,0; see MOLPRO user manual[38]) and an active space of four a_1, two b_1, three b_2, and two a_2 molecular orbitals (i.e., with occ,8,3,6,2; the highest a_1 molecular orbital of a default full valence active space with MOLPRO is excluded), the total numbers of uncontracted and internally contracted configurations in the MRCI calculation are more than 2.5×10^9 and 43.8×10^6, respectively. CASSCF and CASSCF/MRCI calculations of these sizes are the largest that could be handled by the computer systems available to us. Summarizing, it is computationally too demanding to employ a full valence active space in CASSCF/MRCI calculations on YO_2 or YO_2^- using MOLPRO. This is with the MOLPRO default frozen core, where the Y $4s^24p^6$ electrons have already been excluded from the active space. In conclusion, it is simply impractical to correlate the Y $4s^24p^6$ electrons in CASSCF/MRCI calculations on YO_2/YO_2^-. The same applies to the relatively less demanding CASSCF/RSPT2 calculations.

Last, contributions of off-diagonal spin−orbit interaction between the four lowest-lying doublet states of YO_2 to computed T_{vert}'s (vertical excitation energies from the ground electronic state of YO_2) were calculated employing average-state CASSCF/L1 wave functions of the relevant electronic states, as well as a spin−orbit pseudopotential of Y (from the ECP28MDF ECP) and the computed RCCSD(T)/L electronic energies for the spin−orbit diagonal elements. Spin−orbit interaction has not been considered for low-lying quartet states of YO_2 because they were found to be significantly higher in energy than the four lowest doublet states studied (vide infra). Generally, spin−orbit contributions are small (less than 0.003 eV; vide infra) and hence have not been further considered.

Potential Energy Functions, Anharmonic Vibrational Wave Functions and Franck−Condon Factor Calculations. The first photodetachment band of YO_2^-, which arises from the YO_2 ($\tilde{X}^2B_2$) + e ← YO_2^- ($\tilde{X}^1A_1$) detachment process, has been simulated employing computed Franck−Condon (FC) factors. Details of the method employed to calculate FC factors including allowance for Duschinsky rotation and anharmonicity have been described previously[39,40] and hence are not repeated here. Nevertheless, some technical details specific to the calculations of the potential energy functions (PEFs) and anharmonic vibrational wave functions of the $\tilde{X}^1A_1$ state of YO_2^- ($\tilde{X}^2B_2$ state of YO_2) are given. The ranges of the bond length, r(YO), and bond angle, θ(OYO), used in the RCCSD(T)/L energy scans are $1.50 \le r \le 2.55$ Å and $80 \le \theta \le 160°$ ($1.55 \le r \le 2.40$ Å and $85 \le \theta \le 175°$), respectively; 120 (110) RCCSD(T)/L energies were used in the fitting of the PEFs. The root-mean-square (rms) deviations of the fitted PEFs from computed ab initio energies are 6.2 (8.2) cm^{-1}. The vibrational quantum numbers of the harmonic basis functions of the symmetric stretching and bending modes employed in the calculation of anharmonic wave functions have values of up to $v_1'' = 5$ and $v_2'' = 12$ ($v_1' = 8$ and $v_2' = 15$). In addition, restrictions of $(v_1'' + v_2'') \le 12$ $\{(v_1' + v_2') \le 15\}$ have been imposed. The computed RCCSD(T)/L PEFs of the $\tilde{X}^1A_1$ state of YO_2^- and the $\tilde{X}^2B_2$ state of YO_2 and the full list of computed FC factors are available, upon request, from the authors.

Results and Discussions

The $\tilde{X}^1A_1$ State of YO_2^-. Optimized geometrical parameters and computed vibrational frequencies of the $\tilde{X}^1A_1$ state of YO_2^- obtained at different levels of calculation are summarized in Table 2. Information on the frozen core and active space employed in correlated calculations and the computed T_1 diagnostics obtained from CCSD(T) calculations are also given in Table 2 (under remarks; see also footnotes of Table 2). Before these results are discussed, it should be noted that computed CI coefficients of the major electronic configuration obtained from CASSCF and MRCI calculations are larger than 0.94 and 0.90, respectively, indicating that multireference character is negligibly small for the $\tilde{X}^1A_1$ state of YO_2^- at its equilibrium geometry. In this connection, the single-reference CCSD(T) method should be adequate.

From Table 2, it can be seen that the optimized bond lengths, r_e, of the $\tilde{X}^1A_1$ state of YO_2^- obtained in the present study range from 1.940 to 2.021 Å, with a spread of 0.081 Å. These computed r_e values can be considered as reasonably consistent, and hence, it is concluded that computed r_e values of the $\tilde{X}^1A_1$ state of YO_2^- are not very sensitive to the levels of theory used. However, the computed bond angles, θ_e, have values ranging from 112.1 to 135.6°, a spread of 23.5°. In general, DFT values are at the lower end with magnitudes between approximately 112 and 118°. This is especially the case with the BP86 functional which gives values of around 112°, similar to previous DFT results from ref 6 (see Table 2). On the other hand, computed CASSCF, CASSCF/MRCI, and CCSD(T) bond angles, obtained employing the MOLPRO default frozen core of O $1s^2$ and Y $4s^24p^6$ or a larger frozen core, are at the higher end of over 130°, while the CASSCF/RSPT2 values, which range between 125.5 and 133.9°, appear to be rather sensitive to the basis sets and/or the frozen core/active space used. Nevertheless, CCSD(T) and BD(T) θ_e values, which were computed with the Y $4s^24p^6$ electrons correlated, have reasonably consistent values of between 118.3 and 121.4°. This is the case whether the CCSD(T) calculations were carried out using GAUSSIAN03 or MOLPRO and is especially the case with the larger basis sets J, K, and L, which employ the cc-pwCVTZ-PP or cc-pwCVQZ-PP basis set for Y. These weighted core-valence basis sets of Y account for correlation of the Y $4s^24p^6$ electrons more adequately than other basis sets used for Y (such as the earlier Stuttgart RSC basis set and its variants used in basis sets A, F, and C), as mentioned above.

Summing up, it appears that, as long as the Y $4s^24p^6$ electrons are correlated, computed RCCSD(T) bond angles are reasonably consistent and hence are concluded to be reliable. The best theoretical estimate of θ_e of the $\tilde{X}^1A_1$ state of YO_2^- is 120.7° (the CCSD(T)/K value). The computed BD(T)/F bond angle of 119.4° can be considered as agreeing reasonably well with the best theoretical estimate, in view of the fact that basis F is considerably smaller than basis set K. However, the computed BD/F θ_e of 124.5° is clearly too large. Contributions of triple excitation are important, even when Bruckner orbitals are used. Computed DFT bond angles appear to be too small, particularly with the BP86 functional. Regarding multireference methods employed in the present study, as has been commented, it is impractical to include the Y 4s4p shells in the active space. In any case, whether for the multireference methods or the CCSD(T) method used in the present study, it is clear that the exclusion of the Y $4s^24p^6$ electrons in the correlation treatment is the main cause of the large spread of the computed θ_e values. Inspection of the outputs of geometry optimization calculations on the $\tilde{X}^1A_1$ state of YO_2^- reveals that without the Y $4s^24p^6$

TABLE 2: Optimized Geometrical Parameters (r_e in Å and θ_e in °) and Computed Harmonic Vibrational Frequencies {$\omega_1(a_1)$, $\omega_2(a_1)$, and $\omega_3(b_2)$ in cm^{-1}} of the $\tilde{X}^1A_1$ state of YO_2^-

method	r_e	θ_e	ω_e's	remarks[a]
B3LYP/F	1.955	116.7	713,195,620	G03
B98/F	1.948	117.2	727,197,641	G03
BP86/F	1.957	112.1	697,209,599	G03
CCSD(T)/A	1.943	118.3	717,183,605	G03
CCSD(T)/F	1.974	119.0		G03, CCSD max. iteration in freq. calns.
BD/F	1.963	124.5	721,174,645	G03
BD(T)/F	1.973	119.4	689,173,581	G03
B3LYP/H	1.941	118.0		MOLPRO
B88−P86/H	1.941	112.7		MOLPRO
B88−P86/D	1.945	112.7		MOLPRO
CASSCF/H	1.979	135.6		MOLPRO
CAS/RSPT2[b]/B	1.998	131.8		MOLPRO, O $2s^2$ also frozen
CAS/RSPT2[b]/C	1.984	128.2		MOLPRO, O $2s^2$ also frozen
CAS/RSPT2[c]/E	1.976	125.5		MOLPRO, $9a_1$ removed from active space
CAS/RSPT2[c]/H	2.007	133.9		MOLPRO, O $2s^2$ also frozen
CAS/MRCI+D/A	2.007	133.9		MOLPRO, O $2s^2$ frozen, $9a_1$ removed
CAS/MRCI+D/G	2.012	135.2		MOLPRO, O $2s^2$ frozen, $9a_1$ removed
CCSD(T)/B	2.008	130.9		MOLPRO, $T_1 = 0.032$
CCSD(T)/E	2.017	132.4		MOLPRO, $T_1 = 0.030$
CCSD(T)/H	2.021	133.1	640,128,557	MOLPRO, $T_1 = 0.031$
RHF/UCCSD(T)/H	2.021	133.1		MOLPRO, $T_1 = 0.031$, spin contamination = 0.0
CCSD(T)/I	2.019	133.5	639,129,562	MOLPRO, $T_1 = 0.029$
CCSD(T)/A	1.943	118.3	716,180,606	MOLPRO, only O $1s^2$ frozen, $T_1 = 0.035$
CCSD(T)/C	1.958	121.4	696,165,581	MOLPRO, only O $1s^2$ frozen, $T_1 = 0.034$
CCSD(T)/J	1.945	120.9	703,175,590	MOLPRO, all electrons correlated, $T_1 = 0.027$
CCSD(T)/K	1.940	120.7	707,174,596	MOLPRO, only O $1s^2$ frozen, $T_1 = 0.028$
CCSD(T)/L	1.946	120.9	698,171,588	MOLPRO, only O $1s^2$ frozen, $T_1 = 0.029$
CCSD(T)/L, PEF	1.946	120.9	702,172,−	
CCSD(T)/L, ν's			699,171,−	
BP86/LanL2DZ	1.948	109.9	715,216,613	G94; D95* for O (ref 6)
BP86/LanL2DZ	1.962	111.0	701,213,608	G94; 6-31+G* for O (ref 6)
BP86/LanL2DZ	1.965	112.8	702,194,681	G94; 6-311+G(3d) for O (ref 6)
IR matrix		<123[d]	702.0,−,618.6	(ref 6)

[a] The default frozen core for CCSD(T), BD, and BD(T) calculations using G03 consists only the O $1s^2$ electrons. With MOLPRO, the default frozen core consists of O $1s^2$ and Y $4s^24p^6$, and a full valence active space was used for all CASSCF, CASSCF/RSPT2, CASSCF/MRCI, and RCCSD(T) calculations, unless otherwise stated (see text). [b] The RS2 module of MOLPRO with analytical gradients was used. [c] The RSC2 module of MOLPRO for larger systems with numerical gradients was used. [d] The angle upper limit estimated from the O 16/18 isotopic ratio for ν_3'' (b_2); see original work for detail.

electrons being correlated, the bending electronic energy surface is very flat (with very small computed gradients over a wide range of θ values). The computed harmonic bending frequencies obtained without the Y $4s^24p^6$ electrons being correlated [e.g., CCSDD(T)/I ν_2 is 129 cm^{-1}] are also significantly smaller than those with these Y electrons being correlated [e.g., CCSD(T)/K ν_2 is 175 cm^{-1}], supporting the conclusion that without the Y $4s^24p^6$ electrons being correlated, the bending electronic energy surface is very flat.

Comparing results obtained in the present study with available experimental data, the best theoretical estimate of θ_e of 120.7° for the $\tilde{X}^1A_1$ state of YO_2^- is in agreement with an estimated upper limit of 123° derived from the O 16/18 isotope ratio for the asymmetric stretching mode observed in matrix isolation IR spectra (see ref 6). The computed ω_1 values obtained here of between 698 and 716 cm^{-1} at the CCSD(T) level with basis sets A, C, J, K, and L, and the ν_1 value of 699 cm^{-1} obtained from the CCSD(T)/L PEF, agree very well with the experimental ν_1 value of 702.0 cm^{-1} from ref 6. For the asymmetric stretching mode, computed ω_3 values of between 581 and 606 cm^{-1} also agree reasonably well with the experimental ν_3 value of 618.6 cm^{-1} also from ref 6.

The $\tilde{X}^2B_2$ State of YO_2. Optimized geometrical parameters, computed vibrational frequencies, electron affinities (EA), and $<S_2>$ values (for unrestricted-spin wave functions) of, and computed bond angle changes upon detachment ($\Delta\theta_e$) to, the $\tilde{X}^2B_2$ state of YO_2, obtained at different levels of calculations, are summarized in Table 3. First, a lower energy C_S structure (an $^2A'$ state) of YO_2 has also been investigated at the B3LYP/F, B98/F, BP86/F, and CASSCF/H levels of calculation. A similar C_S structure of ScO_2 has been reported and concluded to result from a flat symmetry-breaking potential, but the highest levels of theory give very low effective barriers to interconversion of equivalent C_S minima, low enough that the zero-point vibrational energy lies above the barrier leading to an overall dynamical C_{2V} symmetry (see ref 18 and references therein). Although DFT results obtained here on YO_2 differ in detail with different functionals (e.g., an imaginary asymmetric stretching frequency computed for the C_{2V} structure with B3LYP and B98, but all real computed vibrational frequencies computed with BP86), they agree essentially with the above conclusion of ref 18 on ScO_2 that the C_S and C_{2V} structures are very close in energy as the differences between computed EA values of the C_S and C_{2V} structures of YO_2 are smaller than 0.007 eV with all three functionals used. Regarding CASSCF/H results on both the C_S and C_{2V} structures of YO_2, it appears that they are most likely unreliable, because the computed CASSCF EA values are considerably smaller than those obtained from other methods which account for dynamic electron correlation. Since RCCSD(T) calculations on the $\tilde{X}^2B_2$ state of YO_2 performed in the present study give a true minimum (with all real vibrational frequencies; see Table 3) and the computed harmonic

TABLE 3: Optimized Geometrical Parameters (r_e in Å and θ_e in °), Computed Harmonic Vibrational Frequencies {$\omega_1(a_1)$, $\omega_2(a_1)$, and $\omega_3(b_2)$ in cm^{-1}}, and EA of, and the Computed Change in Bond Angle ($\Delta\theta_e$ in °) upon Electron Detachment to, the $\tilde{X}^2B_2$ State of YO_2

method	r_e	θ_e	ω_e's	EA	$\Delta\theta_e$	remarks[a]
UB3LYP/F	1.932	120.1	688,106,116i	1.939	+3.3	$S^2 = 0.778$
UB3LYP/F	1.872,2.021	114.9	738,84,276	1.937	−1.8	C_s, $^2A'$, $S^2 = 0.771$
UB98/F	1.924	121.9	695,104,162i	1.839	+4.7	$S^2 = 0.779$
UB98/F	1.852,2.039	113.7	756,104,334	1.832	−3.5	C_s, $^2A'$, $S^2 = 0.767$
UBP86/F	1.933	118.9	679,111,484	1.971	+6.8	$S^2 = 0.760$
UBP86/F	1.933,1.934	118.9	679,111,489	1.971	+6.8	C_s, $^2A'$, $S^2 = 0.760$
UCCSD(T)/A	1.912	122.4	723,120,376	1.948	+4.1	$S^2 = 1.043$
UCCSD(T)/F	1.928	121.8	(scf failure)	1.914	+2.8	$S^2 = 1.128$
UBD/F	1.926	126.6	(scf failure)	1.834	+2.1	$S^2 = 1.137$
UBD(T)/F	1.938	123.9	(unrealistic)	1.887	+4.5	$S^2 = 1.703$
UKS-B3LYP/H	1.912	128.7		1.772	+10.8	$S^2 = 0.773$
UKS−B88-P86/H	1.913	126.7		1.900	+14.0	$S^2 = 0.759$
UKS−B88-P86/D	1.921	122.2		1.900	+9.4	$S^2 = 0.761$
CASSCF/H	1.927	150.9		0.785	+15.3	
CASSCF/H	1.832,2.171	119.7		0.153	−15.9	C_s, $^2A'$
CAS/RSPT2/B	1.953	141.6		1.884	+9.8	
CAS/RSPT2/C	1.939	137.7		1.818	+9.5	
CAS/RSPT2/E	unoptimized	(129.1)				CAS not converged
CAS/RSPT2/H	unoptimized	(linear)				
CAS/MRCI+D/A	1.964	141.0		1.956	+7.1	
RCCSD(T)/B	1.958	149.4		2.005	+18.5	$T_1 = 0.034$
RCCSD(T)/E	1.959	162.7		2.032	+30.4	$T_1 = 0.031$
RCCSD(T)/H	1.962	165.9	629,39,665	2.038	+32.7	$T_1 = 0.031$
RHF/UCCSD(T)/H	1.962	165.0		2.020	+31.9	$T_1 = 0.031$, spin cont. = 0.014
RCCSD(T)/I	1.957	169.9	624,26,691	2.082	+36.4	$T_1 = 0.030$
RCCSD(T)/A	1.913	123.2	695,117,431	1.954	+5.0	$T_1 = 0.031$
RCCSD(T)/C	1.921	129.2	678,112,453	1.965	+7.8	$T_1 = 0.031$
RCCSD(T)/J	1.908	131.8	684,121,590	2.025	+10.8	$T_1 = 0.026$
RCCSD(T)/K	1.904	131.5		2.070	+10.8	$T_1 = 0.028$
RCCSD(T)/L	1.909	131.6	681,122,503	2.026	+10.7	$T_1 = 0.029$
RCCSD(T)/L, PEF	1.909	131.4	683,119,−	2.027	+10.5	
RCCSD(T)/L, ν's			680,117,−			
RCCSD(T)/M				2.085		//RCCSD(T)/K; frozen O $1s^2$
extrapolated ($1/X^3$)				2.100		based on RCCSD(T)/K,M
best estimated EA_0				2.09		RCCSD(T)/L ZPE
BP86/LanL2DZ[6]	1.927	115.3	705,112,499	1.778[b]	+5.4	D95* for O
BP86/LanL2DZ[6]	1.939	116.3	682,103,482	1.995[c]	+5.3	6-31+G* for O
BP86/LanL2DZ[6]	1.941	123.2	681,114,503	1.951[d]	+10.4	6-311+G(3d) for O
IR matrix[6]			708.2,−,−			
photodetachment			640(80)	2.00(3)		

[a] See remarks and footnotes given in Table 2 for the program, frozen, and active molecular orbitals used. [b] At 41 kcal·mole^{-1}; see ref 6. [c] At 46 kcal·mole^{-1}; see ref 6. [d] At 45 kcal·mole^{-1}; see ref 6.

b_2 asymmetric stretching frequencies obtained with different basis sets and even with different frozen cores are reasonable and consistently large (>430 cm^{-1}), indicating that the asymmetric stretching electronic energy surface at the RCCSD(T) level of calculation is not flat, the C_S structure of YO_2 has not been further considered.

Second, unrestricted-spin, UCCSD(T), UBD, and UBD(T), calculations gave computed $<S_2>$ values which are considerably larger than 0.75 for the doublet state studied, indicating large spin contaminations with the corresponding unrestricted-spin wave functions. In addition, the UCCSD(T)/F and UBD/F numerical derivative vibrational frequency calculations failed with SCF failures, and UBD(T)/F frequency calculations gave unrealistic results (see Table 3). Summing up, in view of the large spin contaminations associated with unrestricted-spin wave functions of the $\tilde{X}^2B_2$ state of YO_2, it is concluded that unrestricted-spin methods are unsuitable for the investigation of this neutral state.

Third, some CASSCF/RSPT2 geometry optimization calculations did not converge; the CASSCF/RSPT2/E optimization stopped at $\theta = 129.1°$ because of CASSCF convergence failure, while the CASSCF/RSPT2/H optimization was converging toward a near-linear geometry (Table 3). In general, CASSCF/RSPT2 geometry optimizations show a very flat bending electronic energy surface for the $\tilde{X}^2B_2$ state of YO_2, similar to what was found for the $\tilde{X}^1A_1$ state of YO_2^-. Consequently, the computed optimized bond angles have a wide range of values because they are very sensitive to the basis sets used to obtain them, as shown in Table 3. Also, we just mention that CASSCF/MRCI/G geometry optimization calculations were carried out but did not converge, with the bond angle moving between 120 and 169° in an oscillatory manner. Similar to the conclusion made above for the $\tilde{X}^1A_1$ state of YO_2^-, when the Y $4s^24p^6$ electrons are not correlated in these multireference calculations, the bending electronic energy surface of the $\tilde{X}^2B_2$ state of YO_2 is very flat.

Finally, we focus on the RCCSD(T) results. Also similar to what was found for the $\tilde{X}^1A_1$ state of YO_2^- discussed above, when the Y $4s^24p^6$ electrons are not correlated in the RCCSD(T) calculations, the bending electronic surface of the $\tilde{X}^2B_2$ state of YO_2 is very flat, resulting in a wide range of computed optimized bond angles (between ∼149° with the basis set B

and ~170° with basis set I; Table 3). In addition, the computed bending vibrational frequencies obtained without the Y $4s^24p^6$ electrons being correlated have very small values [39 and 26 cm^{-1} at the RCCSD(T)/H and RCCSD(T)/I levels of calculation, resectively; see Table 3], supporting this conclusion. However, when the Y $4s^24p^6$ electrons are correlated, the computed optimized bond angles have values between 123.2° with basis set A and ~131.5° with basis sets J, L, and K. With the latter, larger basis sets J, L, and K, cc-pwCVXZ-PP basis sets were used for Y, which have tight sets of functions to account for the explicit correlation of the Y $4s^26p^6$ electrons, and they gave very consistent computed bond angles for the $\tilde{X}^2B_2$ state of YO_2, with values converging to ~131.5°. The relatively small computed θ_e value of 123.2° obtained with basis A is almost certainly because the Stuttgart RSC basis set in its contracted form is inadequate for the explicit correlation of the Y $4s^24p^6$ electrons. With basis set C, which has the Stuttgart RSC basis set of Y uncontracted, a larger optimized bond angle of 129.2° is obtained because the uncontracted form of the Stuttgart RSC basis set gave a better description of the Y $4s^24p^6$ electrons than that for the contracted form as used in basis set A. Summarizing, it is clear that adequate correlation of the Y $4s^24p^6$ electrons is vital in obtaining a reliable minimum-energy geometry for the $\tilde{X}^2B_2$ state of YO_2. This is also the case when the computed bond angle changes upon photodetachment from the $\tilde{X}^1A_1$ state of YO_2^- to the $\tilde{X}^2B_2$ state of YO_2 ($\Delta\theta_e$ in Table 3) are considered. Consistent $\Delta\theta_e$ values of around 10.8° have been obtained only when the larger basis sets, J, L, and K, which employed cc-pwCVXZ-PP type basis sets for Y, were used and the Y $4s^24p^6$ electrons were correlated.

Last, we consider the computed vibrational frequencies obtained by the RCCSD(T) method. Correlating the Y $4s^24p^6$ electrons also gave computed bending frequencies which are considerably larger in value (~120 cm^{-1}; Table 3) than those without the explicit correlation of these electrons, supporting the conclusion made regarding the importance of the explicit correlation of the Y $4s^24p^6$ electrons. Regarding the computed RCCSD(T) harmonic frequencies of the asymmetric stretching mode (ω_3), they are real and reasonably large in magnitude, particularly with the larger and better basis sets J and L. In addition, the computed RCCSD(T)/A ω_3 value of 431 cm^{-1} is considerably larger than the corresponding UCCSD(T)/A value of 376 cm^{-1}, suggesting that Hartree−Fock instability and/or symmetry breaking in the asymmetric stretching coordinate, if present, most likely arise from effects associated with spin contamination. Regarding the computed symmetric stretching frequencies (ω_1 and ν_1), they range between 678 and 695 cm^{-1} (considering only values obtained when the Y $4s^24p^6$ electrons were correlated; see Table 3), and values of ~680 cm^{-1} obtained employing the larger basis sets J and L should be more reliable. These computed values for the $\tilde{X}^2B_2$ state of YO_2 agree reasonably well with the available experimental values of 708.2 and 640 ± 80 cm^{-1} obtained from the matrix IR spectrum[6] of YO_2 and the photodetachment spectrum[11] of YO_2^-, respectively.

Computed Electron Affinity of YO_2. From the computed electron affinities (EAs) of YO_2 obtained at different levels of calculation shown in Table 3, it is clear that the CASSCF method, which does not account for dynamic electron correlation, performs poorly, as mentioned above briefly. Although most other methods, which account for dynamic electron correlation to various extents, gave computed EA values which are fairly close to the experimental value of 2.00 ± 0.03 eV, such apparently good agreement may be fortuitous for some of these methods, in view of the large variations in the computed

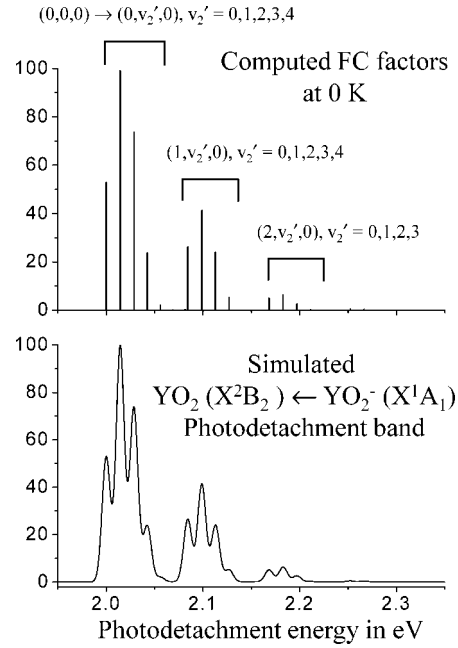

Figure 1. Computed Franck−Condon (FC) factors, vibrational designations of some major vibrational progressions (top trace), and the simulated YO_2 ($\tilde{X}^2B_2$) ← YO_2^- ($\tilde{X}^1A_1$) photodetachment band of YO_2^- (bottom trace) at a Boltzmann vibrational temperature of 0 K.

$\Delta\theta_e$ values obtained and discussed above. On the basis of conclusions drawn from the above discussions on the optimized geometrical parameters and computed vibrational frequencies of the $\tilde{X}^1A_1$ state of YO_2^- and the $\tilde{X}^2B_2$ state of YO_2, we focus only on the more reliable RCCSD(T) results, which have the Y $4s^24p^6$ electrons properly correlated. In this connection, further single-energy RCCSD(T)/M//RCCSD(T)/K calculations were carried out on both the $\tilde{X}^1A_1$ state of YO_2^- and the $\tilde{X}^2B_2$ state of YO_2 in order to obtain a more reliable EA value of YO_2. The EA values obtained at the RCCSD(T)/K (core-valence quadruple-ζ quality for Y and augmented valence quadruple-ζ quality for O) and RCCSD(T)/M (corresponding quintuple-ζ quality) levels were then used for the extrapolation to the complete basis set (CBS) limit employing the $1/X^3$ formula.[41] The CBS value obtained is 2.10 eV. Uncertainties of ±0.02 eV have been estimated based on the difference between the CBS and RCCSD(T)/M values. Including zero-point vibrational energy correction employing the computed RCCSD(T)/L harmonic vibrational frequencies, the best theoretical EA_0 value is estimated to be 2.09 ± 0.02 eV, which compares reasonably well with the experimental value of 2.00 ± 0.03 eV from ref 11.

Computed Franck−Condon Factors and Simulated Photodetachment Band. Computed Franck−Condon (FC) factors and the corresponding photodetachment band of the YO_2 ($\tilde{X}^2B_2$) + e ← YO_2^- ($\tilde{X}^1A_1$) process are shown in Figure 1 (top and bottom traces, respectively). They were obtained with a Boltzmann vibrational temperature of 0 K (i.e., without "hot" bands). The experimental EA value of 2.00 eV has been used for the (0,0,0) ← (0,0,0) position in the simulated spectrum. Each vibrational component of the simulated spectrum (bottom trace in Figure 1) has been simulated with the corresponding computed FC factor (the vibrational component with the maximum computed FC factor is set to 100 arbitrary units in the figure) and a Gaussian line shape with a full-width at half-maximum (fwhm) of 10 meV. The spectral resolution of 10 meV (80 cm^{-1}) fwhm has been used in order for the vibrational structure in the bending mode of the $\tilde{X}^2B_2$ state of YO_2 with the computed fundamental frequency of 117 cm^{-1} to be resolved

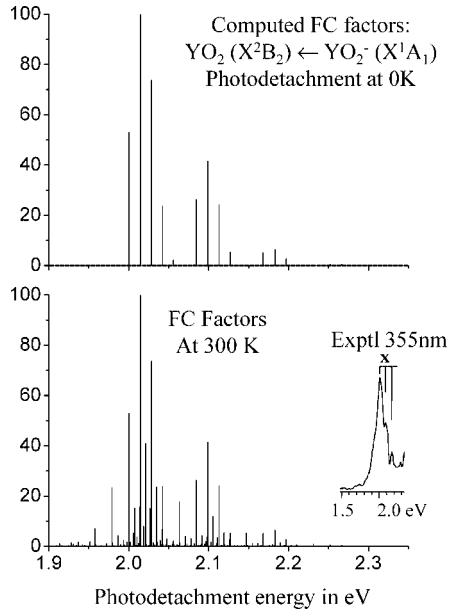

Figure 2. Computed Franck−Condon (FC) factors of the YO_2 ($\tilde{X}^2B_2$) ← YO_2^- ($\tilde{X}^1A_1$) photodetachment at a Boltzmann vibrational temperature of 0 (top trace) and 300 K (bottom trace) with the relevant part of the experimental 355 nm photodetachment spectrum from ref 11 inserted (bottom right); see text and Figure 3 for the vibrational designations of the "hot" bands.

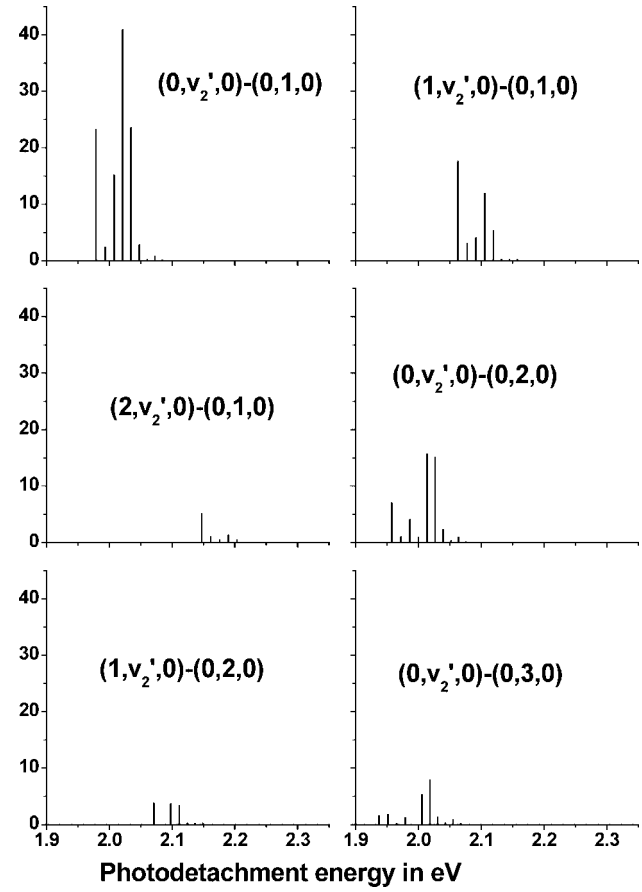

Figure 3. Computed Franck−Condon factors of some major "hot" band series at a Boltzmann vibrational temperature of 300 K and their vibrational designations [note that the full scale of the *y* axes have been set to 45 arbitrary units; this corresponds to the (0,1,0) ← (0,0,0) vibrational component being set to 100 arbitrary units in Figures 1and 2].

in the simulated spectrum. It should also be noted that, although the experimental resolution of the reported 355 nm photodetachment spectrum of YO_2^- of ref 11 has a considerably larger fwhm than 10 meV, recent research on instrumentation of photoelectron and/or photodetachment spectroscopy shows that meV electron energy resolution is achievable.[42–44] A Gaussian line shape was used to simulate each vibrational component because, from experience, a Gaussian line shape corresponds well with the experimental one.

According to the computed FC factors, the assignment of the major vibrational series of this photodetachment band can be established and is given in the top trace of Figure 1. It can be seen that there are three to four combination bands involving both the symmetric stretching and bending modes of the $\tilde{X}^2B_2$ state of YO_2. This is in line with the computed bond length and angle changes upon detachment of approximately −0.037 Å and +10.7° at the RCCSD(T)/L level. As shown in Figure 1, the first and strongest combination band is the $(0,v_2',0)$ ← (0,0,0) series, with $v_2' = 0, 1, 2, 3, 4, \ldots$. The first vibrational component in this combination band is the (0,0,0) ← (0,0,0) transition, and it has an appreciable computed FC factor (0.529, when that of the strongest vibrational component is set to 1.0). The second component, (0,1,0) ← (0,0,0,), has the largest computed FC factor. The whole photodetachment band ends effectively at a detachment energy of ∼2.3 eV.

The portion of the experimental 355 nm photodetachment spectrum from ref 11, which is relevant to the present study, is shown in Figure 2 (inserted bottom right of Figure 2). The vibrational structure of the experimental spectrum only shows three to four components, which were assigned to the symmetric stretching mode of the $\tilde{X}^2B_2$ state of YO_2, and no vibrational structure of the bending mode is resolved because the experimental resolution of 30 meV (242 cm^{-1}) fwhm (at 1 eV kinetic energy)[11] is unable to resolve a vibrational spacing of ∼120 cm^{-1} of the ν_2 bending mode of the $\tilde{X}^2B_2$ state of YO_2. In addition, there appears to be a rising background toward higher detachment energy underneath of the first photodetachment band. When this rising background is considered in the comparison between the simulated (Figure 1 bottom trace) and observed (Figure 2 inserted bottom right) spectra, it can be concluded that they agree very well. Such a good agreement between theory and experiment provides strong support for the assignments of the molecular carrier of, electronic states involved and vibrational structure of, the YO_2 (∼X^2B_2) + e ← YO_2^- (∼X^1A_1) photodetachment band reported in ref 11. In addition, it is concluded that the RCCSD(T)/L PEFs employed to calculate the FC factors are reliable, and the computed geometry change upon detachment to the $\tilde{X}^2B_2$ state of YO_2 is very close to the true one.

Although no resolvable "hot" bands have been identified in the observed first band of the 355 and 266 nm photodetachment spectra of YO_2^- reported in ref 11, it is not uncommon for vibrationally and/or electronically "hot" anions to be produced in the anion source used in a typical photodetachment experiment as that of ref 11. (Note that some spectral features in the photodetachment spectra of ScO_2^- have been attributed to "hot" bands in ref 11.) In this connection, FC factors were also computed for the YO_2 ($\tilde{X}^2B_2$) + e ← YO_2^- ($\tilde{X}^1A_1$) photodetachment process with a YO_2^- Boltzmann vibrational temperature of 300 K, and they are plotted in the bottom trace of Figure 2 (with those at 0 K in the upper trace, in order to more clearly show contributions from "hot" bands). Computed FC factors show that "hot" bands arising from photodetachment from the (0,1,0), (0,2,0), (0,3,0), (0,4,0), and (1,0,0) levels of the $\tilde{X}^1A_1$ state of YO_2^- have appreciable contributions. The computed

TABLE 4: Computed Vertical Excitation Energies [in eV; from the $\tilde{X}^2B_2$ State at RCCSD(T)/L-Optimized Geometry of the $\tilde{X}^2B_2$ State], Major Electronic Configurations (Open-Shell Molecular Orbitals) and Their Computed CI Coefficients (in Parentheses from CASSCF Calculations), and T_1 Diagnostics [in Squared Brackets from RCCSD(T) Calculations] of Low-Lying Electronic States of YO_2 Obtained at Different Levels of Calculations

state; conf.[a]	CAS[b]/L	CAS[c]/L	CAS[c]/L1	RCCSD[d]/L	RCCSD(T)[d]/L
$^2A_1$; $(6a_1)^1$	1.16 (0.932)	1.20 (0.922)	1.11[e] (0.931)	0.714 [0.0271]	0.745
$^2B_1$; $(2b_1)^1$	1.36 (0.932)	1.40 (0.933)	1.30 (0.931)	0.916 [0.0264]	0.949
$^2A_2$; $(1a_2)^1$	2.07 (0.922)	2.10 (0.914)	2.01[f] (0.925)	1.666 [0.0285]	1.635
$^2A_1$; $(5a_1)^1(6a_1)^2$				2.064 [0.0438]	1.878
$^4B_2$; $(6a_1)^1(7a_1)^1(5b_2)^1$	2.18 (0.973)	2.60 (0.827)		2.416 [0.027]	2.967
$^4A_2$;	2.49				
$(7a_1)^1(2b_1)^1(5b_2)^1$	(0.817)				
$(6a_1)^1(7a_1)^1(1a_2)^1$	(0.526)				
$^4B_1$;	2.70				
$(7a_1)^1(5b_2)^1(1a_2)^1$	(0.765)				
$(6a_1)^1(7a_1)^1(5b_2)^1$	(−0.603)				
$^4A_1$;	2.71				
$(7a_1)^1(5b_2)^1(6b_2)^1$	(0.760)				
$(6a_1)^1(7a_1)^1(5b_2)^1$	(0.609)				

[a] With the ECP28MDF ECP for Y, the electronic configuration of the $\tilde{X}^2B_2$ state of YO_2 is $...(6a_1)^2(2b_1)^2(5b_2)^1(1a_2)^2$. The open-shell molecular orbitals of the low-lying doublet and quartet states are shown. For the four doublet excited states shown, the $5b_2$ molecular orbital is doubly occupied. [b] Single-state CASSCF calculations for each state with the O 2p and Y 4d and 5s shells active (i.e.; with closed,4,1,3,0; see MOLPRO manual and text). [c] Average-state CASSCF calculations for all states shown with the O 2p and Y 4d and 5s shells active (i.e.; with closed,4,1,3,0; see MOLPRO manual and text). [d] Only frozen O $1s^2$ electrons (i.e., with core,1,0,1,0; see MOLPRO manual). [e] The computed transition dipole moment between this state and the $\tilde{X}^2B_2$ state is 0.1228 Debye. [f] The computed transition dipole moment between this state and the $\tilde{X}^2B_2$ state is 0.0102 Debye.

TABLE 5: Optimized Geometrical Parameters (r_e and θ_e in Å and °, Respectively), Computed Relative Electronic Energies (T_e and T_{vert} in eV; Relative to, and from, the $\tilde{X}^2B_2$ State of YO_2, Respectively), Adiabatic Electron Affinities (EA in eV; Relative to $\tilde{X}^1A_1$ State of YO_2^-), Vertical Detachment Energies (VDEs in eV; from the $\tilde{X}^1A_1$ State of YO_2^-), and the Corresponding Computed T_1 Diagnostics (in Parentheses) of the Low-Lying Doublet States of YO_2 Obtained at the RCCSD(T)/L Level of Calculation

YO_2	$\tilde{X}^2B_2$	$\tilde{A}^2A_1$	$\tilde{B}^2B_1$	$\tilde{C}^2A_2$
r_e	1.909	1.910	1.969	1.970
θ_e	131.6	113.9	118.3	105.2
T_e (RCCSD)	0	0.585	0.812	1.199
T_e {RCCSD(T)}	0	0.573	0.787	1.111
T_{vert} (RCCSD)	0	0.714 (0.027)	0.916 (0.026)	1.666 (0.029)
T_{vert} {RCCSD(T)}	0	0.745	0.949	1.635
T_{vert} {RCCSD(T) + SO}	0[b]	0.745	0.951	1.635
EA (RCCSD)	2.05 (0.029)	2.63 (0.028)	2.86 (0.029)	3.25 (0.032)
EA {RCCSD(T)}	2.03	2.60	2.81	3.14
VDE (RCCSD)	2.13 (0.031)	2.67 (0.029)	2.86 (0.029)	3.38 (0.030)
VDE {RCCSD(T)}	2.07	2.63	2.83	3.29
VDE (experimental)[11]	2.00(3)	2.46(9)[a]	2.75(5)[a]	3.28(6)

[a] The assignments of these two states from the photodetachment study are $\tilde{A}^2B_1$ and $\tilde{B}^2A_1$, based on a comparison with VO_2 (see original work). Our calculations revised these assignments as shown (see text). [b] The spin−orbit ECP of ECP28MDF, average-state CASSCF wave functions (with basis L1) of the four doublet states shown in this table, and their corresponding computed RCCSD(T)/L energies (for the diagonal elements of the spin−orbit matrix) were used in the spin−orbit interaction calculation. Off-diagonal spin−orbit coupling lowers the $\tilde{X}^2B_2$ state of YO_2 by 5.1 cm^{-1}.

FC factors of the main "hot" band series are plotted in Figure 3, together with their vibrational designations. The strongest "hot" band series is the $(0,v_2',0) \leftarrow (0,1,0)$ series, with the (0,3,0) ← (0,1,0) component at a photodetachment energy of 2.02 eV having the strongest computed FC factor in this series [a computed FC factor of 0.409, with the FC factor of the overall, strongest (0,1,0) ← (0,0,0) component set to 1.0]. As can be seen from Figure 3, other "hot" band series are considerably weaker. The "hot" bands at a Boltzmann vibrational temperature of 300 K contribute essentially as a shoulder, at a lower detachment energy, of the main $(0,v_2',0) \leftarrow (0,0,0)$ band. The contributions of "hot" bands obtained at a Boltzmann temperature of 300 K to the YO_2 ($\tilde{X}^2B_2$) + e ← YO_2^- ($\tilde{X}^1A_1$) photodetachment band actually yield an even better agreement between theory and experiment.

Low-Lying Excited States of YO_2. Results from further calculations on low-lying electronic states of YO_2 are summarized in Tables 4 and 5. First, computed vertical excitation energies to low-lying quartet states obtained at the CASSCF/L, CASSCF/L1, and RCCSD(T)/L levels (Table 4) show that these quartet states are considerably higher in energy than low-lying doublet states in the vertical excitation region, and hence, quartet states have not been further considered.

Second, computed CI coefficients from CASSCF calculations and T_1 diagnostics from RCCSD(T) calculations, as shown in Table 4, suggest that multireference character is negligibly small for the lowest $^2A_1$, $^2B_1$, and $^2A_2$ states in the vertical excitation region from the $\tilde{X}^2B_2$ state of YO_2. Therefore, a single-reference method, such as RCCSD(T), should be adequate for these low-lying doublet states of YO_2.

Third, optimized geometrical parameters and computed relative electronic energies, including adiabatic excitation energies (T_e) and vertical excitation energies (T_{vert}) of, and EAs and vertical detachment energies (VDEs) to, low-lying doublet states

of YO_2 from the $\tilde{X}^2B_2$ state of YO_2 and the $\tilde{X}^1A_1$ state of YO_2^-, respectively, obtained at the RCCSD(T)/L level of calculation are summarized in Table 5. On the basis of the computed T_e values shown in Table 5, the first excited state of YO_2 is the $\tilde{A}^2A_1$ state, followed by the $\tilde{B}^2B_1$ and $\tilde{C}^2A_2$ states. Their T_e and T_{vert} values reported here will be useful for the future assignment of the absorption and/or LIF spectra of YO_2, when they are recorded.

Last, the computed VDE values to the $\tilde{X}^2B_2$ and $\tilde{C}^2A_2$ states of YO_2 agree very well with the corresponding experimental values obtained from the photodetachment spectrum of YO_2^- reported in ref 11 (see Table 5). The computed VDE values to the $\tilde{A}^2A_1$ and $\tilde{B}^2B_1$ states are larger than the corresponding experimental values by 0.17 and 0.08 eV, respectively. Nevertheless, in view of the uncertainties of ± 0.09 and ± 0.05 eV associated with these experimental values given in ref 11 (see Table 5) and also the fact that the VDE position of a spectral band depends on the FC factors, it can be concluded that the agreements between the theoretical and experimental VDE values of these two detachment bands are reasonably good. In this connection, on the basis of the computed VDEs, the assignments of the second and third photodetachment bands of YO_2^- are revised to the detachments to the $\tilde{A}^2A_1$ and $\tilde{B}^2B_1$ states of YO_2, respectively, instead of the $\tilde{A}^2B_1$ and $\tilde{B}^2A_1$ states given in ref 11. However, the differences between the computed EA and VDE values and the predicted geometry changes upon detachments to these two electronic states of YO_2 are rather small ($\sim$0.03 eV and less than 0.036 Å and 7°, respectively), suggesting that the detachment bands to these two states should not be broad. This is contrary to the broad spectral features observed in the 2.3 to 3.0 eV region of the 355 nm photodetachment spectrum of YO_2^- reported and assigned to the detachments from the $\tilde{X}^1A_1$ state of YO_2^- to the $\tilde{A}^2B_1$ and $\tilde{B}^2A_1$ states of YO_2 in ref 11. On the basis of our ab initio results, it seems very likely that there are contributions from other detachment processes to spectral features underneath the photodetachment bands to these two electronic states of YO_2.

Concluding Remarks

A variety of DFT and ab initio calculations have been carried out on the $\tilde{X}^1A_1$ state of YO_2^- and the $\tilde{X}^2B_2$ state of YO_2. Although the computed EAs obtained from these calculations, except CASSCF calculations, which lack dynamic electron correlation, agree reasonably well with the experimental value measured from the photodetachment spectrum of YO_2^-, the optimized bond angles of both the $\tilde{X}^1A_1$ state of YO_2^- and the $\tilde{X}^2B_2$ state of YO_2 and their predicted changes upon detachment have wide ranges of values. With the CASSCF/RSPT2, CASSCF/MRCI, and RCCSD(T) methods, it was found that, when the Y $4s^24p^6$ electrons are not correlated, the bending electronic energy surfaces of both neutral and anionic electronic states studied are very flat, resulting in a wide range of computed equilibrium bond angles. Nevertheless, with the RCCSD(T) method, when the Y $4s^24p^6$ electrons are correlated, especially using a core-valence basis set which accounts for these outer-core electrons of Y adequately, consistent and reliable results have been obtained.

In order to check further the reliability of the computational method employed, Franck−Condon factors, using a method which includes allowance of anharmonicity and Duschinsky rotation, were computed employing RCCSD(T)/ECP28MDF_aug-cc-pwCVTZ, aug-cc-pVTZ potential energy functions (with the Y $4s^24p^6$ electrons correlated). Computed FC factors and the simulated spectrum of the YO_2 ($\tilde{X}^2B_2$) + e ← YO_2^- ($\tilde{X}^1A_1$) detachment process were compared with the 355 nm experimental photodetachment spectrum.[11] The excellent agreement obtained confirms the reliability of the RCCSD(T) method in the investigation of the YO_2^-/YO_2 systems.

On the basis of the reliable RCCSD(T) results, it is concluded that DFT results, at least with the three functionals employed in the present study, are unreliable. In addition, for the closed-shell $\tilde{X}^1A_1$ state of YO_2^-, although the BD(T) results, which agree with the RCCSD(T) results (both with the Y $4s^24p^6$ electrons correlated), are reliable, the BD results are unreliable. Moreover, for the open-shell $\tilde{X}^2B_2$ state of YO_2, unrestricted-spin methods, including the CCSD(T), BD, and BD(T) method, were found to be unreliable because of large spin contaminations. Regarding calculations employing multireference (MR) methods, CASSCF, CASSCF/RSPT2, and CASSCF/MRCI, it is computationally too demanding to include the Y $4s^24p^6$ electrons in the active space. Consequently, these MR methods are concluded to be impractical for the YO_2^-/YO_2 systems.

Some low-lying doublet excited states of YO_2 have also been studied. Their EAs and VDEs have been calculated and used to assist assignment of the 355 nm photodetachment spectrum of YO_2^-.[11] On the basis of computed RCCSD(T) VDE values, previous assignments of the second and third photodetachment bands of YO_2^- have been revised. Also, on the basis of the differences between computed EA and VDE values and predicted geometry changes, it is concluded that spectral features observed in the 2.3− 3.0 eV region of the published photodetachment spectrum of YO_2^- are not solely due to the detachments from the $\tilde{X}^1A_1$ state of YO_2^- to the $\tilde{A}^2A_1$ and $\tilde{B}^2B_1$ states of YO_2. For the photodetachment spectra of ScO_2, spectral features have been attributed to photodetachments of vibrationally and/or electronically excited anions (see ref 11 for detail). Finally, we have also calculated T_e and T_{vert} of the $\tilde{A}^2A_1$, $\tilde{B}^2B_1$, and $\tilde{C}^2A_2$ states of YO_2, which will be useful for future assignments of their absorption and/or LIF spectra, when they are recorded.

Acknowledgment. The authors are grateful to the Research Committee of the Hong Kong Polytechnic University of HKSAR (Grant Numbers A-PA8U and A-PG14) and the Research Grant Council (RGC) of the Hong Kong Special Administrative Region (HKSAR; Grant Number PolyU 5014/06) for financial support. The provision of computational resources from the EPSRC (U.K.) National Service for Computational Chemistry Software is also acknowledged.

References and Notes

(1) Padmanabhan, P. V. A.; Ramanathan, S.; Sreekumar, K. P.; Satpute, R. U.; Kutty, T. R. G.; Gonal, M. R.; Gantayet, L. M. *Mater. Chem. Phys.* **2007**, *106*, 416.

(2) Pires, A. M.; Serra, O. A.; Davolos, M. R. *J. Lumin.* **2005**, *113*, 174.

(3) Al-Yassir, N.; Le Van Mao, R. *Appl. Catal., A* **2007**, *317*, 275.

(4) Gruber, J. B.; Sardar, D. K.; Nash, K. L.; Yow, R. M. *J. Appl. Phys.* **2007**, *102*, 023103.

(5) Lee, C. K.; Kim, W. S.; Park, H.-H; Jeon, H.; Pae, Y. H. *Thin Solid Films* **2005**, *473*, 335.

(6) Andrews, L.; Zhou, M. F.; Chertihin, G. V.; Bauschlicher, C. W. *J. Phys. Chem. A* **1999**, *103*, 6525.

(7) Dai, B; Deng, K. M.; Yang, J. L. *Chem. Phys. Lett.* **2002**, *364*, 188.

(8) Gu, G. Y.; Dai, B.; Ding, X. L.; Yang, J. L. *Eur. Phys. J. D* **2004**, *29*, 27.

(9) Knickelbein, M. *J. Chem. Phys.* **1995**, *102*, 1.

(10) Kang, W. Y.; Bernstein, E. R. *Bull. Korean Chem. Soc.* **2005**, *26*, 345.

(11) Wu, H.; Wang, L.-S. *J. Phys.Chem. A* **1998**, *102*, 9129.

(12) Pramann, A.; Nakamura, Y.; Nakajima, A.; Kaya, K. *J. Phys. Chem. A* **2005**, *105*, 7534.

(13) Knight, L. B.; Babb, R.; Ray, M.; Banisaukas, T. J.; Russon, L.; Daily, R. S.; Davidson, E. R. *J. Chem. Phys.* **1966**, *105*, 10237.

(14) Rosi, M.; Bauschlicher, C. W.; Chertilin, G. V.; Andrews, L. *Theor. Chim. Acta* **1998**, *99*, 106.

(15) Bauschlicher, C. W., Jr.; Zhou, M.; Andrews, L.; Johnson, J. R. T.; Panas, I.; Snis, A.; Roos, B. O. *J. Phys. Chem. A* **1999**, *103*, 5463.

(16) Gutsev, G. L.; Rao, B. K.; Jena, P. *J. Phys. Chem. A* **2000**, *104*, 11961.

(17) Gonzales, J. M.; King, R. A.; Schaefer, H F. *J. Chem. Phys.* **2000**, *113*, 567.

(18) Kim, S.-J.; Crawford, T. D. *J. Phys. Chem. A* **2004**, *108*, 3097.

(19) Peterson, K. A.; Figgen, D.; Dolg, M.; Stoll, H. *J. Chem. Phys.* **2007**, *126*, 124101.

(20) See also the Stuttgart website, http://www.theochem.uni-stuttgart.de/pseudopotentials/clickpse.en.html.

(21) Dolg, M.; Wedig, U.; Stoll, H.; Preuss, H. *J. Chem. Phys.* **1987**, *86*, 866.

(22) Andrae, D.; Haeussermann, U.; Dolg, M.; Stoll, H.; Preuss, H. *Theor. Chim. Acta* **1990**, *77*, 123.

(23) Martin, J. M. L.; Sundermann, A. *J. Chem. Phys.* **2001**, *114*, 3408.

(24) Becke, A. D. *Phys. Rev. A* **1988**, *38*, 3098.

(25) Perdew, J. P. *Phys. Rev. B* **1986**, *33*, 8822.

(26) Schmider, H. L.; Becke, A. D. *J. Chem. Phys.* **1998**, *108*, 9624.

(27) Werner, H.-J.; Knowles, P. J. *J. Chem. Phys.* **1985**, *82*, 5053.

(28) Werner, H.-J. *Mol. Phys.* **1996**, *89*, 645.

(29) Celani, P.; Werner, H.-J. *J. Chem. Phys.* **2000**, *112*, 5546.

(30) Werner, H.-J.; Knowles, P. J.; Lindh, R.; Manby, F. R.; Schütz, M.; Celani, P.; Korona, T.; Rauhut, G.; Amos, R. D.; Bernhardsson, A.; Berning, A.; Cooper, D. L.; Deegan, M. J. O.; Dobbyn, A. J.; Eckert, F.; Hampel, C.; Hetzer, G.; Lloyd, A. W.; McNicholas, S. J.; Meyer, W.; Mura, M. E.; Nicklass, A.; Palmieri, P.; Pitzer, R.; Schumann, U.; Stoll, H.; Stone, A. J.; Tarroni, R.; Thorsteinsson, T. *MOLPRO*, a package of ab initio programs; 2006.

(31) Werner, H.-J.; Knowles, P. J. *J. Chem. Phys.* **1988**, *89*, 5803.

(32) (a) Knowles, P. J.; Hampel, C.; Werner, H.-J. *J. Chem. Phys.* **1993**, *99*, 5219. (b) Knowles, P. J.; Hampel, C.; Werner, H.-J. *J. Chem. Phys.* **2000**, *112*, 3106.

(33) Watts, J. D.; Gauss, J.; Bartlett, R. J. *J. Chem. Phys.* **1993**, *98*, 8718.

(34) Scuseria, G. E.; Schaefer, H. F. *J. Chem. Phys.* **1989**, *90*, 3700.

(35) Pople, J. A.; Head-Gordon, M.; Raghavachari, K. *J. Chem. Phys.* **1987**, *87*, 5968.

(36) Handy, N. C.; Pople, J. A.; Head-Gordon, M.; Raghavachari, K.; Trucks, G. W. *Chem. Phys. Lett.* **1989**, *164*, 185.

(37) Frisch, M. J. Trucks, G. W.; Schlegel, H. B.; Scuseria, G. E.; Robb, M. A.; Cheeseman, J. R.; Montgomery, J. A.; Jr Vreven, T.; Kudin, K. N.; Burant, J. C.; Millam, J. M.; Iyengar, S. S.; Tomasi, J.; Barone, V.; Mennucci, B.; Cossi, M.; Scalmani, G.; Rega, N.; Petersson, G. A.; Nakatsuji, H.; Hada, M.; Ehara, M.; Toyota, K.; Fukuda, R.; Hasegawa, J.; Ishida, M.; Nakajima, T.; Honda, Y.; Kitao, O.; Nakai, H.; Klene, M.; Li, X.; Knox, J. E.; Hratchian, H. P.; Cross, J. B.; Bakken, V.; Adamo, C.; Jaramillo, J.; Gomperts, R.; Stratmann, R. E.; Yazyev, O.; Austin, A. J.; Cammi, R.; Pomelli, C.; Ochterski, J. W.; Ayala, P. Y.; Morokuma, K.; Voth, G. A.; Salvador, P.; Dannenberg, J. J.; Zakrzewski, V. G.; Dapprich, S.; Daniels, A. D.; Strain, M. C.; Farkas, O.; Malick, D. K.; Rabuck, A. D.; Raghavachari, K.; Foresman, J. B.; Ortiz, J. V.; Cui, Q.; Baboul, A. G.; Clifford, S.; Cioslowski, J.; Stefanov, B. B.; Liu, G.; Liashenko, A.; Piskorz, P.; Komaromi, I.; Martin, R. L.; Fox, D. J.; Keith, T.; Al-Laham, M. A.; Peng, C. Y.; Nanayakkara, A.; Challacombe, M.; Gill, P. M. W.; Johnson, B.; Chen, W.; Wong, M. W.; Gonzalez, C.; Pople, J. A. *Gaussian 03*,revision C.02; Gaussian, Inc.: Wallingford, CT, 2004.

(38) MOLPRO website. http://www.molpro.net/.

(39) Mok, D. K. W.; Lee, E. P. F.; Lee; Chau, F.-t.; Wong, D. C.; Dyke, J. M. *J. Chem. Phys.* **2000**, *113*, 5791.

(40) Chau, F.-t.; Mok, D. K. W.; Lee, E. P. F.; Dyke, J. M. *ChemPhysChem* **2005**, *6*, 2037.

(41) Halkier, A.; Helgaker, T.; Klopper, W.; Jorgensen, P.; Csaszar, A. G. *Chem. Phys. Lett.* **1999**, *310*, 385.

(42) Giniger, R.; Hippler, T.; Ronen, S.; Cheshnovsky, O. *Rev. Sci. Instrum.* **2001**, *72*, 2543.

(43) Osterwalder, A.; Nee, M. J.; Zhou, J.; Neumark, D. M. *J. Chem. Phys.* **2004**, *121*, 6317.

(44) Klar, D.; Ruf, M.-W.; Fabrikant, I. I.; Hotop, H. *J. Phys. B: At. Mol. Opt. Phys.* **2001**, *34*, 3855.

JP711948R